Published in final edited form as:
*Clin Cancer Res*. 2010 August 1; 16(15): 3910–3922. doi:10.1158/1078-0432.CCR-10-0005.

# Targeted Gene Silencing Using RGD-Labeled Chitosan Nanoparticles

**Hee Dong Han**[1], **Lingegowda S. Mangala**[1], **Jeong Won Lee**[1,2], **Mian M.K. Shahzad**[1,3], **Hye Sun Kim**[1,4], **Deyu Shen**[1], **Eun Ji Nam**[1,5], **Edna M. Mora**[6,7,8], **Rebecca L. Stone**[1], **Chunhua Lu**[1], **Sun Joo Lee**[1,9], **Ju Won Roh**[1,10], **Alpa M. Nick**[1], **Gabriel Lopez-Berestein**[11,12,13,14], and **Anil K. Sood**[1,12,13,14]

[1]Department of Gynecologic Oncology, The University of Texas M.D. Anderson Cancer Center, Houston, TX

[2]Department of Obstetrics and Gynecology, Samsung Medical Center, Sungkyunkwan University School of Medicine, Seoul, Korea

[3]Department of Obstetrics and Gynecology, Baylor College of Medicine, Houston, TX

[4]Department of Pathology, Cheil General Hospital and Women's Healthcare Center, Kwandong University College of Medicine, Seoul, Korea

[5]Women's Cancer Clinic, Department of Obstetrics and Gynecology, Yonsei University College of Medicine, Seoul, Korea

[6]Department of Surgical Oncology, The University of Texas M.D. Anderson Cancer Center, Houston, TX

[7]Department of Surgery, School of Medicine, University of Puerto Rico, San Juan, Puerto Rico

[8]University of Puerto Rico Comprehensive Cancer Center, San Juan, Puerto Rico

[9]Department of Obstetrics and Gynecology, Konkuk University Hospital, Konkuk University School of Medicine, Seoul, Korea

[10]Department of Obstetrics & Gynecology, Dongguk University IIsan Hospital, Goyang, South Korea

[11]Department of Experimental Therapeutics, The University of Texas M.D. Anderson Cancer Center, Houston, TX

[12]Department of Cancer Biology, The University of Texas M.D. Anderson Cancer Center, Houston, TX

[13]Center for RNA Interference and Non-coding RNA, The University of Texas M.D. Anderson Cancer Center

## Abstract

**Purpose—**To develop an Arg-Gly-Asp (RGD) peptide-labeled chitosan nanoparticle (RGD-CH-NP) as a novel tumor targeted delivery system for siRNA.

Correspondence should be addressed to: Anil, K. Sood, M.D., Departments of Gynecologic Oncology and Cancer Biology, Unit 1362, P.O. Box 301439, University of Texas M. D. Anderson Cancer Center, Houston, TX 77230-1439, Phone: 713-745-5266; Fax: 713-792-3643, asood@mdanderson.org.
[14]Joint Senior Authors

**Experimental Design—**RGD peptide conjugated with CH by thiolation reaction was confirmed by H-NMR. Binding of RGD-CH-NP with αvβ3 integrin was examined by flow cytometry and fluorescence microscopy. Antitumor efficacy was examined in orthotopic mouse models of ovarian carcinoma.

**Results—**We demonstrate that RGD-CH-NP loaded with siRNA significantly increased selective intratumoral delivery in orthotopic animal models of ovarian cancer. In addition, we demonstrate targeted silencing of multiple growth promoting genes (POSTN, FAK, and PLXDC1) along with therapeutic efficacy in the SKOV3ip1, HeyA8, and A2780 models using siRNA incorporated into RGD-CH-NP (siRNA/RGD-CH-NP). Furthermore, we demonstrate *in vivo* tumor vascular targeting using the RGD-CH-NP by delivering PLXDC1-targeted siRNA into the αvβ3 integrin positive tumor endothelial cells in the A2780 tumor-bearing mice. This approach resulted in significant inhibition of tumor growth compared to controls.

**Conclusions—**This study demonstrates that RGD-CH-NP is a novel and highly selective delivery system for siRNA with the potential for broad applications in human desease.

### Keywords

RNA interference; RGD; αvβ3 integrin; chitosan nanoparticle; ovarian carcinoma

**Translational Relevance**

We have developed a novel method for linking the RGD peptide to chitosan nanoparticles (RGD-CH-NP) to increase selective delivery of siRNA. In addition, we demonstrate targeted silencing of multiple growth promoting genes along with therapeutic efficacy in orthotopic animal models of ovarian carcinoma. RGD-CH-NP is a novel and highly selective delivery system for siRNA with the potential for broad applications in human disease.

## Introduction

RNA interference (RNAi)-based approaches hold great potential for cancer therapy (1-3). SiRNA-based therapy may allow development of a broad armamentarium of targeted drugs against genes that are difficult to target with other traditional approaches such as small molecules or monoclonal antibodies. However, one of the key challenges to the use of siRNA for therapy is the need for efficient intracellular delivery because unprotected siRNA is rapidly cleared or degraded by nucleases. Delivery of siRNA across plasma membranes *in vivo* has been achieved using delivery systems such as liposomes (4-6), nanoparticles(7-9) and chemically modified siRNA (1). Although these delivery approaches have been shown to be effective in pre-clinical models, many cannot be used in clinical settings due to non-specific delivery, which may lead to unwanted or unexpected side effects. Therefore, to overcome these limitations, novel delivery systems are needed. A desirable delivery system should lead to enhanced concentrations of therapeutic payloads at disease sites, minimize concerns about off-target effects (3), and ultimately raise the therapeutic index. Chitosan is particularly attractive for clinical and biological applications due to its low immunogenicity, low toxicity, and biocompatibility (10,11). In addition to its advantages such as protonated amine groups, chitosan can increase binding efficiency with cells because of electrostatic interactions (12).

For a targeted delivery system (3,8,13), various receptors on the tumor cell surface have been established as a target binding site to achieve selective delivery. One such protein receptor of interest is the αvβ3 integrin, which has been considered for selective delivery

(14-17). The αvβ3 integrin is overexpressed in a wide range of tumors, and is largely absent in normal tissues, which is a desirable feature for selective delivery. Here, we developed a cyclic Arg-Gly-Asp (RGD) peptide-labeled chitosan nanoparticle (RGD-CH-NP) for tumor targeted delivery of siRNA. The cyclic RGD has one or two ring structures, and provides conformation stability and improved binding selectivity for the αvβ3 integrin. Moreover, cyclic peptides are less susceptible to biodegradation than linear RGD peptides (18,19). In the current study, we demonstrate highly selective delivery of targeted nanoparticles to αvβ3 integrin expressing cells and the therapeutic efficacy of this approach in multiple ovarian cancer models.

## Materials and Methods

### Conjugation of RGD and CH

Conjugation of RGD (c[RGDfK (Ac-$SCH_2CO$)], MW 719.82 Da) and CH (MW 50-190 KDa) is shown in Fig. 1A. The RGD and CH were conjugated by thiolation reaction using cross-linking reagent, N-succinimidyl 3-(2-pyridyldithio)-propionate (SPDP). Briefly, 10.5 ml of 2 mg/ml CH solution (1% acetate buffer) was added to 700 μg of SPDP to react $NH_2$ group of the CH for 4 hr at room temperature. After that, 500 μg of RGD was added to SPDP-activated CH solution for 24 hr at room temperature. After this reaction, dialysis was performed for 48 hr to isolate conjugates. The conjugates were confirmed by H-NMR (CH and CH-RGD: 1% acetic acid included $D_2O$, RGD: DMSOd6, 500 MHz, HRMAS-FT-NMR, Bruker, Germany). In addition, to determine the RGD concentration in RGD-CH-NPs, RGD peptide was labeled with FITC as shown in Supplementary Fig. S1 (20).

### Preparation of siRNA/RGD-CH-NP

RGD-CH-NP was prepared based on ionic gelation of anionic TPP and siRNA. Briefly, predetermined TPP (0.25% w/v) and siRNA (1 μg/μL) were added in RGD-CH solution, and the siRNA/RGD-CH-NP were spontaneously formed under constant stirring at room temperature. After incubation at 4 °C for 40 min, siRNA/RGD-CH-NP was collected by centrifugation (Thermo Biofuge, Germany) at 13,000 rpm for 40 min at 4 °C. The pellet was washed by sterile water 3 times to isolate siRNA/RGD-CH-NP, which was stored at 4 °C until used.

### Characteristics of siRNA/RGD-CH-NP

The RGD concentration in the RGD-CH-NPs was calculated by measuring FITC intensity based on a calibration curve of standard concentration of FITC-labeled with RGD by a fluorescence spectrophotometer (20). Size and zeta potential of RGD-CH-NP were measured by light scattering with a particle size analyzer and Zeta Plus (Brookhaven Instrument Co., CA), respectively. Co-incorporation of FITC-labeled RGD and Alexa555 siRNA into siRNA/RGD-CH-NP was observed by fluorescence microscopy, and the physical morphology of siRNA/RGD-CH-NP was observed by SEM.

### Cell lines and siRNA

The derivation and source of the human epithelial ovarian cancer cell lines SKOV3ip1, HeyA8, A2780, A2780ip2, and murine ovarian endothelial cells (MOEC) have been previously described (4,5,21). The POSTN siRNA (target sequence: 5′-GGAUCUUGUGGCCCAAUUA-3′), FAK siRNA (target sequence: 5′-CCACCUGGGCCAGUAUUAU-3′), PLXDC1 siRNA (target sequence: 5′GACACCUGCGUCCUCGA-3′), and control siRNA (target sequence: 5′-UUCUCCGAACGUGUCACGU-3′) were purchased from Sigma (USA)(22).

### Binding of RGD-CH-NPs

To confirm the *in vitro* binding efficiency of RGD-CH-NP against αvβ3 integrin on the cell surface, we conducted both flow cytometry analysis and fluorescence microscopy. To measure binding efficiency of Alexa555 siRNA/RGD-CH-NP, cells were incubated for 20 min at 4 °C after NPs were added, and then cells were collected by centrifugation (1,500 rpm, 3 min). The binding efficiency was measured by flow cytometry (23,24). To observe cell binding of RGD-CH-NP, cells were fixed in a chamber slide using 4% paraformaldehyde and then the cells were stained with Hoechst 33258 for 10 min at 4 °C (to stain nuclei blue) and observed under fluorescence microscopy (magnification ×200) (23,24). In addition, we confirmed intracellular delivery of CH-NP or RGD-CH-NP by confocal microscopy. Briefly, we added CH-NP or RGD-CH-NP in cells and then incubated for 20 min at room temperature. After that, cells were fixed using 4% paraformaldehyde and then the cells were stained with sytox green (to stain nuclei green) for 10 min at room temperature and observed under confocal microscopy. To confirm binding of RGD-CH-NP by tumor cells, morphology of the cells was observed by TEM (23,24).

### *In vivo* delivery of siRNA/RGD-CH-NP

Detection of uptake of Alexa555 siRNA/RGD-CH-NP was performed as described previously (25,26). Relevant tissues were harvested after single injection of either control siRNA/CH-NP, Alexa555 siRNA/CH-NP or Alexa555 siRNA/RGD-CH-NP into SKOV3ip1-bearing mice. Uptake efficiency was determined by the percentage of Alexa555 siRNA-labeled NPs location into tissue in 5 random fields at ×200 magnification for each tumor and organ. In addition, to confirm αvβ3 integrin-mediated delivery of RGD-CH-NP, we performed αvβ3 integrin staining in tumor tissues as described above.

### Western blot analysis

The preparation of cultured cell lysates and tumor tissue lysates has been previously described (5,27). Protein concentrations were determined using a BCA Protein Assay Reagent Kit (Pierce Biotech., Rockford, IL) and aliquots of 20 μg protein were subjected to gel electrophoresis on 7.5% or 10% SDS-PAGE gels. Transfer to membranes and immunoblotting was performed as described previously (28).

### Orthotopic *in vivo* model of ovarian cancer and tissue processing

Female athymic nude mice (NCr-nu) were purchased from the National Cancer Institute-Frederick Cancer Research and Development Center (Frederick, MD) and maintained as previously described (29). All mouse studies were approved by the M. D. Anderson Cancer Center Institutional Animal Care and Use Committee. The mice used for *in vivo* experiments were 8 to 12 weeks old. To produce tumors, SKOV3ip1, HeyA8, and A2780 ($1 \times 10^6$ cells per 0.2 ml HBSS) cells were injected into the peritoneal cavity (i.p.) of mice. Mice (n= 10 per group) were monitored daily for adverse effects of therapy and were sacrificed when any of the mice seemed moribund.

To assess tumor growth, treatment began 1 week after i.p. injection of tumor cells into mice. Each siRNA-incorporated CH-NP or RGD-CH-NP was given twice weekly at a dose of 150 μg/kg body weight through i.v injection. Docetaxel was diluted in PBS and injected i.p once a week, at a dose of 100 μg in 200 μl. Treatment continued until mice became moribund (typically 4 to 5 weeks depending on tumor-cell). Mouse weight, tumor weight, number of nodules, and distribution of tumors in mice were recorded at the time of sacrifice. The individuals who performed the necropsies, tumor collections, and tissue processing were blinded to the treatment group assignments. Tissue specimens were fixed either with

formalin or OCT (optimum cutting temperature; Miles, Inc., Elkhart, IN) or were snap frozen.

### Real time quantitative RT-PCR

Relative expression of POSTN and FAK mRNA in mice after treatment was determined by real-time quantitative RT-PCR using 50 ng total RNA isolated from treated tumor tissue using the RNeasy Mini Kit (Qiagen). Relative expression values were obtained using the $2^{-\Delta\Delta CT}$ method, and normalized to control for percent fold changes (30).

### Immunohistochemical staining

Immunohistochemical (IHC) analysis was performed on tumor tissue from mice that were treated by i.v. injection of siRNA/CH-NP or siRNA/RGD-CH-NP. Procedures for IHC analysis of cell proliferation (Ki67), microvessel density (CD31), and POSTN expression (POSTN antibody) were performed as described previously (27,31). All of these analyses were recorded in 5 random fields for each slide at ×100 magnification. In addition, terminal deoxynucleotidyl transferase-mediated nick end labeling (TUNEL) was performed as described previously to determine cell apoptosis (32). The quantification of apoptotic cells was calculated by the number of apoptotic cells in 5 random fields at ×200 magnification. All staining was quantified by 2 investigators in a blinded fashion.

### Statistical analysis

Differences in continuous variables were analyzed using the student's t test for comparing two groups and ANOVA was performed to compare differences for multiple group comparisons. For values that were not normally distributed, the Mann-Whitney rank sum test was used. The statistical package for the Social Sciences (SPSS, Inc.) was used for all statistical analyses. A $p$ value of $<0.05$ was considered statistically significant.

## Results

### Characteristics of siRNA incorporated RGD-CH-NPs (siRNA/RGD-CH-NP)

In this study, we selected the αvβ3 integrin as a target receptor since it is selectively expressed in a large proportion of ovarian cancer cells and associated tumor vasculature. Therefore, we utilized a well-characterized targeting peptide, Arg-Gly-Asp (RGD), which can bind specifically to the αvβ3 integrin (33,34). We first conjugated the RGD peptide with CH by thiolation reaction of SPDP (Fig. 1A) and the conjugates were confirmed by H-NMR analysis (Supplementary Fig. S2). As shown in Supplementary Fig. S2C, the peaks for the CH of benzene group in RGD (1) and $CH_2$ of methylene in RGD (1.5 ppm) (2) were observed at 7-8 ppm and 1-2 ppm, respectively. Additionally, conjugation of RGD with CH and CH-NP was measured using FITC-labeled RGD by fluorescence intensity (Supplementary Fig. S1). Conjugation yield of RGD with CH is up to 60% (data not shown) and RGD concentration on RGD-CH-NP was determined by measuring FITC intensity based on a calibration curve of standard concentration of FITC-labeled with RGD.

Based on conjugation of RGD-CH, RGD-CH-NPs were prepared. We prepared 5 different siRNA/RGD-CH-NPs with varying amounts of RGD (Fig. 1B). The size and zeta potential of siRNA/RGD-CH-NPs were around 200 nm and 40 mV, respectively (Fig. 1B). The histogram of RGD-CH-NP 5 is shown in Supplementary Fig. S3. These experiments indicate that RGD conjugation with CH-NP does not affect formation and physicochemical properties of siRNA/RGD-CH-NPs. Additionally, the incorporation of RGD and siRNA into RGD-CH-NP 5 was confirmed by fluorescence microscopy using FITC-labeled RGD (green) and Alexa555-labeled siRNA (red) (Fig. 1C, upper panel). The morphology of

siRNA/RGD-CH-NP 5 was determined by scanning electron microscopy (SEM). The particles were spherical in shape and the size was around 200 nm (Fig. 1C, lower panel).

### RGD-CH-NP enhances binding efficiency on αvβ3 integrin expressing tumor cells

We first assessed the expression of αvβ3 integrin in ovarian cancer cell lines by flow cytometry. While A2780ip2 cells were negative, the SKOV3ip1 cells showed positive expression on the cell membrane against the αvβ3 integrin (Fig. 2A). We next studied the binding efficiency of siRNA/RGD-CH-NPs in both cell lines with different concentrations of RGD (Fig. 1B). As expected, little binding was observed in A2780ip2 cells at any of the 5 different formulations tested (Fig. 2B). However, in the αvβ3 positive SKOV3ip1 cells, binding increased in a RGD concentration dependent manner. Among the five formulations, the siRNA/RGD-CH-NP 5 (1.45 μg RGD/mg chitosan) showed the highest binding (Fig. 2B). Therefore, we selected siRNA/RGD-CH-NP 5 for subsequent experiments. We next confirmed binding efficiency of Alexa555-labeled (Alexa555) siRNA/RGD-CH-NP by fluorescence microscopy against tumor cells. Alexa555 siRNA/RGD-CH-NP showed higher binding efficiency (94.25% induction vs CH-NP) in the SKOV3ip1 cells compared to non-RGD labeled CH-NP. In contrast, similar binding efficiency was observed in the A2780ip2 cells between RGD-CH-NP and CH-NP (Fig. 2C). To observe binding of the RGD-CH-NP in tumor cells, we utilized TEM. In the SKOV3ip1 cells, the RGD-CH-NP showed higher binding compared to the αvβ3-negative A2780ip2 cells (Fig. 2D). In addition, we observed intracellular delivery of CH-NP or RGD-CH-NP using confocal microscopy. Alexa555 siRNA/RGD-CH-NP resulted in higher intracellular efficiency in the SKOV3ip1 cells compared to non-RGD labeled CH-NP (Supplementary Fig. S4).

### RGD-CH-NP enhances targeted delivery to tumor tissues

Prior to performing proof-of-concept *in vivo* efficacy studies, we tested the extent of *in vivo* delivery following a single intravenous injection of Alexa555 siRNA/RGD-CH-NP into SKOV3ip1-bearing mice after 48 hr. The siRNA was observed in >80% of fields examined, and demonstrated up to 3-fold higher localization into tumor tissues compared to CH-NP (Fig. 3A). Additionally, we also stained harvested tumors for the αvβ3 integrin to evaluate co-localization. The Alexa555 siRNA/RGD-CH-NP (red) consistently showed co-localization (yellow) with the αvβ3 integrin (green) in tumor tissues (Fig. 3B). In contrast, delivery with siRNA/CH-NP demonstrated Alexa555 positive siRNA in both αvβ3 positive and negative cells. These findings indicate that siRNA/RGD-CH-NPs indeed result in selective delivery into αvβ3 positive cells. We also examined other organs including liver, kidney, spleen, lung, heart and brain for delivery of siRNA using either the CH-NP or RGD-CH-NP. However, minimal siRNA RGD-CH-NP was observed in these organs as compared to CH-NP due to the greater binding specificity for RGD-CH-NP in tumor tissues (Fig. 3C).

### Therapeutic efficacy of gene silencing with targeted RGD-CH-NP

To determine the effectiveness of gene silencing and potential therapeutic efficacy, we focused on targeting periostin (POSTN), which plays a significant role in cell invasion, survival, and angiogenesis, leading to increased metastasis of cancer cells (35). The SKOV3ip1 and A2780 models were selected for these experiments as they have increased POSTN levels (Supplementary Fig. S5). Following a single intravenous injection of POSTN siRNA/RGD-CH-NP (150 μg siRNA/kg body weight) into SKOV3ip1-bearing mice, tumors were harvested. POSTN expression was reduced by >51% in RGD-CH-NP treated tumors compared to control siRNA/CH-NP and by >20% compared to CH-NP at 24 hr (Fig. 4A). On the basis of this result, we evaluated POSTN expression by immunohistochemstry (IHC) analysis. Delivery of POSTN siRNA with RGD-CH-NP resulted in significantly greater inhibition of POSTN expression in tumor tissues as compared to POSTN siRNA/CH-NP or control siRNA/CH-NP at 24 hr (Fig. 4B).

We next examined the therapeutic efficacy of POSTN silencing with POSTN siRNA/RGD-CH-NP in mice bearing orthotopic SKOV3ip1 (αvβ3 positive) or A2780 (αvβ3 negative) tumors. Seven days following injection of tumor cells into the peritoneal cavity, mice were randomly allocated to the following groups (n=10 mice/group): 1) control siRNA/CH-NP + PBS, 2) POSTN siRNA/CH-NP + PBS, 3) POSTN siRNA/RGD-CH-NP + PBS, 4) control siRNA/CH-NP + docetaxel, 5) POSTN siRNA/CH-NP + docetaxel and 6) POSTN siRNA/RGD-CH-NP + docetaxel. All mice were sacrificed when animals in any group appeared moribund (4 to 5 weeks after cell injection depending on the cell line). In the SKOV3ip1 model, POSTN siRNA/RGD-CH-NP + PBS resulted in significant inhibition of tumor growth compared to POSTN siRNA/CH-NP + PBS (24% reduction; $p < 0.04$) and control siRNA/CH-NP + PBS (71% reduction, $p < 0.001$). Notably, combination of POSTN siRNA/RGD-CH-NP + docetaxel showed the greatest inhibition of tumor growth compared to control siRNA/CH-NP + docetaxel (32% reduction, $p < 0.006$) and CH-NP + docetaxel (22% reduction, $p < 0.01$; Fig. 5A). After treatment, the decrease in POSTN mRNA level was confirmed by qRT-PCR (Fig. 5A). In the A2780 model, POSTN siRNA/RGD-CH-NP + PBS showed significant inhibition of tumor growth compared to control siRNA/CH-NP + PBS (73% reduction, $p < 0.01$), however, POSTN siRNA/RGD-CH-NP + PBS showed no additional benefit compared to POSTN siRNA/CH-NP + PBS ($p < 0.22$; Fig. 5B). As above, decrease in POSTN mRNA level was confirmed by qRT-PCR (Fig. 5B). There were no differences in total body weight, feeding habits or behavior between the groups, suggesting that there were no overt toxicities related to therapy.

To determine potential mechanisms underlying the efficacy of siRNA/RGD-CH-NP therapy in tumor tissues, we examined tumors for markers of cell proliferation (Ki67), microvessel density (MVD, CD31), and apoptosis (TUNEL). In the SKOV3ip1 model, POSTN siRNA/RGD-CH-NP + PBS showed significant inhibition of cell proliferation ($p < 0.001$ vs control siRNA/CH-NP + PBS; $p < 0.05$ vs POSTN siRNA/CH-NP + PBS), MVD ($p < 0.001$ vs control siRNA/CH-NP + PBS; $p < 0.01$ vs POSTN siRNA/CH-NP + PBS), and increased apoptosis ($p < 0.001$ vs control siRNA/CH-NP + PBS; $p < 0.002$ vs POSTN siRNA/CH-NP + PBS). The combination group of POSTN siRNA/RGD-CH-NP + docetaxel had significantly reduced cell proliferation ($p < 0.05$) and MVD ($p < 0.001$), and increased apoptosis as compared to the single treatment groups ($p < 0.001$, Fig. 5C). In the A2780 model, POSTN siRNA/RGD-CH-NP + docetaxel showed significant inhibition of cell proliferation ($p < 0.003$), MVD ($p < 0.001$), and increased cell apoptosis compared to control siRNA/CH-NP + PBS ($p < 0.004$). As expected, neither POSTN siRNA/RGD-CH-NP nor POSTN siRNA/CH-NP showed any significant effects on cell proliferation ($p < 0.10$) and apoptosis ($p < 0.33$, Supplementary Fig. S6A).

To establish that the effects of RGD-CH-NP are not unique to just one target, we also performed *in vivo* experiments with siRNA against additional targets. We targeted FAK due to its prominent role in ovarian cancer growth and progression (36). The HeyA8 cells are both αvβ3 integrin and FAK positive (37). Mice were randomly allocated to one of following 6 groups (n=10 mice/group): 1) control siRNA/CH-NP + PBS, 2) FAK siRNA/CH-NP + PBS, 3) FAK siRNA/RGD-CH-NP + PBS, 4) control siRNA/CH-NP + docetaxel, 5) FAK siRNA/CH-NP + docetaxel and 6) FAK siRNA/RGD-CH-NP + docetaxel. Treatment with FAK siRNA/RGD-CH-NP + PBS resulted in significant inhibition of tumor growth as compared to FAK siRNA/CH-NP + PBS ($p < 0.04$) and control siRNA/CH-NP + PBS ($p < 0.001$, Fig. 5D). Combination of FAK siRNA/RGD-CH-NP + docetaxel resulted in the greatest effect on tumor growth compared to the other single treatment groups ($p < 0.02$) and FAK siRNA/CH-NP + PBS ($p < 0.01$, Fig. 5D). After treatment, FAK mRNA levels (by qRT-PCR) were found to be significantly lower in the FAK siRNA treated groups (Fig. 5D). Treatment with FAK siRNA/RGD-CH-NP + docetaxel resulted in significant inhibition of cell proliferation ($p < 0.05$), MVD ($p < 0.01$), and increased cell apoptosis ($p < 0.01$). The

combination group of FAK siRNA/RGD-CH-NP + docetaxel showed even further decreases in cell proliferation ($p$ <0.001) and MVD ($p$ <0.03), and increased apoptosis compared to the single treatment group ($p$ < 0.04, Supplementary Fig. S6B).

### RGD-CH-NP targets tumor vasculature

Since the αvβ3 integrin is known to be selectively expressed in the tumor vasculature, we also selected PLXDC1, a target we recently identified as being upregulated in ovarian cancer vasculature (38). We first confirmed that the mouse ovarian endothelial cells (*in vitro*) and mouse origin tumor vasculature in A2780 tumor tissue (*in vivo*) express the αvβ3 integrin even though the A2780 cells were negative for αvβ3 integrin expression (Supplementary Fig. S7A and B). As expected, the A2780 tumors harvested from mice lacked αvβ3 expression on tumor cells; however, it was clearly present in tumor vasculature compared to the corpus luteum in the mouse ovary (Supplementary Fig. S7B). Prior to *in vivo* experiments, we confirmed delivery of Alexa555 siRNA/RGD-CH-NP into the tumor vasculature after injection into A2780-bearing mice. Alexa555 siRNA/RGD-CH-NP showed co-localization (yellow) with endothelial cells (CD31, green) in the tumor vasculature compared to CH-NP (Supplementary Fig. S7C). We next carried out experiments with siRNA targeting PLXDC1 (38), which was incorporated into RGD-CH-NP. For these experiments, A2780 tumor bearing mice were randomly allocated to one of the following 3 groups (n=10 mice/group): 1) control siRNA/CH-NP, 2) PLXDC1 siRNA/CH-NP, and 3) PLXDC1 siRNA/RGD-CH-NP. Treatment with PLXDC1 siRNA/RGD-CH-NP resulted in significant inhibition of tumor growth compared to control siRNA/CH-NP (87% reduction; $p$ <0.001, Fig. 6A). The targeted delivery of PLXDC1 siRNA with RGD-CH-NP resulted in even greater efficacy compared to PLXDC1 siRNA with CH-NP ($p$ <0.01, Fig. 6A). Since the A2780 cells lack αvβ3 integrin expression, these results suggest that the RGD-mediated CH-NP targeting is highly effective in targeting the tumor vasculature. We next examined the effects of PLXDC1 gene silencing on the tumor vasculature. PLXDC1 siRNA/RGD-CH-NP resulted in increased apoptosis in the tumor vasculature compared to PLXDC1 siRNA/CH-NP (Fig. 6B). Additionally, to confirm PLXDC1 silencing in the tumor vasculature following PLXDC1 siRNA/RGD-CH-NP injection into A2780-bearing mice, we performed dual immunofluorescence (IF) staining for endothelial cells (CD31, red) and PLXDC1 (green). The PLXDC1 siRNA/RGD-CH-NP treated group resulted in complete PLXDC1 silencing in the tumor vasculature compared to PLXDC1 siRNA/CH-NP (Fig. 6C).

## Discussion

We demonstrate here that a novel receptor-targeted delivery system (RGD-CH-NP) loaded with siRNA targeted to key ovarian cancer associated genes leads to potent anti-tumor efficacy in ovarian carcinoma. This approach has broad utility for selectively targeting tumor cells as well as the associated endothelial cells. The RGD-CH-NP was effective in silencing multiple targets of interest and in achieving therapeutic efficacy.

RNAi-based cancer therapy is a highly specific method of gene silencing, but hurdles related to systemic *in vivo* delivery of siRNA need to be overcome to realize its full potential in clinical settings. Moreover, delivery efficiency of free siRNA without the use of a nanoparticle is quite low and most of the free siRNA is rapidly degraded following intravenous injection (5,39). Therefore, to overcome this limitation, selective targeted delivery systems are needed. While a number of nanoparticle systems have been utilized for therapeutic applications, most of these are widely distributed in the body, and could lead to undesirable toxicities in normal tissues. In addition, wide drug distribution may require higher doses for gene silencing in the target tissue of interest. Therefore, to overcome these limitations against conventional passive delivery, targeted delivery is highly desirable.

Targeted delivery systems have been designed to increase or facilitate uptake into target tissue (3), and to protect siRNA payloads and inhibit nonspecific delivery (3). Recent work comparing non-targeted and targeted nanoparticles has shown that the primary role of the targeting ligands is to enhance selective cellular uptake into cancer cells and to minimize accumulation in normal tissues (40). The addition of targeting ligands that provide specific nanoparticle-cell surface interactions can play a vital role in the ultimate location of nanoparticles. For example, nanoparticles can be targeted to cancer cells if their surfaces contain moieties such as peptides, proteins or antibodies. These moieties can bind with cancer cell-surface receptor proteins such as transferring (41) or folate (42) receptors, which are known to be increased in number on a wide range of cancer cells. These targeting ligands enable nanoparticles to bind to cell-surface receptors and penetrate cells by receptor-mediated endocytosis. However, a limited number of nanoparticle systems have reached clinical development (40).

Nanoparticles can carry a large payload of drugs as compared to antibody conjugates (40,43). Furthermore, nanoparticle payloads are frequently located within the particles, and their type and number may not affect the pharmacokinetics and biodistribution of the nanoparticles. This is unlike molecular conjugates in which the type and number of therapeutic entities conjugated to the targeting ligand significantly modifies the overall properties of the conjugate.

Several synthetic materials have been proposed for effective non-viral siRNA delivery systems such as lipid-based particles, oligofectamine, cyclodextrin, polyethyleneimine, and cholesterol (3). Although many types of compounds have potential utility as delivery agents, some have concerns regarding safety. For example, toxicity of cationic lipid particles has been reported both *in vitro* and *in vivo* (44,45), and some synthetic agents have been found to induce a gene signature of their own that might increase the off-target effects of siRNA (46,47). Therefore, development of siRNA therapeutics for cancer treatment requires clinically suitable, safe and effective drug delivery systems.

Chitosan nanoparticles (CH-NP) have been recently developed for siRNA delivery (12,48,49). Chitosan is an attractive nanoparticle for siRNA delivery because its positive charge allows transport across cellular membranes and subsequent endocytosis. Moreover, chitosan is biodegradable, biocompatible, and has low immunogenicity (10,12,48). Chitosan nanoparticles without a therapeutic payload have no effect on tumor growth compared to untreated animals (50). The αvβ3 integrin is known to be overexpressed in most cancer cells and the tumor vasculature (33,37,51). The αvβ3 integrin is a family of cell surface receptors, which plays an important role in tumor biology and may serve as a useful target (13). In addition to its role in cell matrix recognition, the αvβ3 integrin has been a focus for drug delivery strategies since it assists with internalization and gene transfer (33). In the current study, we developed and characterized RGD-CH-NP incorporated with siRNA as an αvβ3 integrin-targeted delivery system because of its high affinity and highly specific binding. Indeed, our targeted delivery-mediated gene silencing significantly enhanced anti-tumor therapeutic efficacy compared to a non-targeted delivery system in preclinical ovarian cancer models. While the RGD ligand can be useful for binding to integrin family members, additional targeting approaches may be useful. Nevertheless, the targeted delivery strategy presented here has broad potential as a delivery platform in human disease and could be adapted for other targeting ligands.

## Supplementary Material

Refer to Web version on PubMed Central for supplementary material.

## Acknowledgments

The authors thank Nicholas B. Jennings and Donna Reynolds for their technical expertise. We also thank Drs. Robert Langley and Michael Birrer for helpful discussions. Portions of this work were supported by NIH grants (CA 110793, 109298, and RC2GM 092599), DOD (OC-073399, W81XWH-10-1-0158), the Ovarian Cancer Research Fund, Inc. (Program Project Development Grant), U. T. M. D. Anderson Cancer Center SPORE in ovarian cancer (P50CA083639), the Zarrow Foundation, the Medlin Foundation, and the Betty Anne Asche Murray Distinguished Professorship. AMN and RS are supported by NCI-DHHS-NIH T32 Training Grant (T32 CA101642). MMS was supported by the Baylor WRHR grant (HD050128) and the GCF Molly-Cade ovarian cancer research grant.

## References

1. Aagaard L, Rossi JJ. RNAi therapeutics: principles, prospects and challenges. Adv Drug Deliv Rev 2007;59(2-3):75–86. [PubMed: 17449137]
2. Merritt WM, Lin YG, Han LY, et al. Dicer, Drosha, and outcomes in patients with ovarian cancer. N Engl J Med 2008;359(25):2641–50. [PubMed: 19092150]
3. Whitehead KA, Langer R, Anderson DG. Knocking down barriers: advances in siRNA delivery. Nat Rev Drug Discov 2009;8(2):129–38. [PubMed: 19180106]
4. Merritt WM, Lin YG, Spannuth WA, et al. Effect of interleukin-8 gene silencing with liposome-encapsulated small interfering RNA on ovarian cancer cell growth. J Natl Cancer Inst 2008;100(5): 359–72. [PubMed: 18314475]
5. Halder J, Kamat AA, Landen CN Jr, et al. Focal adhesion kinase targeting using in vivo short interfering RNA delivery in neutral liposomes for ovarian carcinoma therapy. Clin Cancer Res 2006;12(16):4916–24. [PubMed: 16914580]
6. Thaker PH, Han LY, Kamat AA, et al. Chronic stress promotes tumor growth and angiogenesis in a mouse model of ovarian carcinoma. Nat Med 2006;12(8):939–44. [PubMed: 16862152]
7. Zhang C, Jugold M, Woenne EC, et al. Specific targeting of tumor angiogenesis by RGD-conjugated ultrasmall superparamagnetic iron oxide particles using a clinical 1.5-T magnetic resonance scanner. Cancer Res 2007;67(4):1555–62. [PubMed: 17308094]
8. Pirollo KF, Chang EH. Targeted delivery of small interfering RNA: approaching effective cancer therapies. Cancer Res 2008;68(5):1247–50. [PubMed: 18316585]
9. Wolfrum C, Shi S, Jayaprakash KN, et al. Mechanisms and optimization of in vivo delivery of lipophilic siRNAs. Nat Biotechnol 2007;25(10):1149–57. [PubMed: 17873866]
10. Han HD, Song CK, Park YS, et al. A chitosan hydrogel-based cancer drug delivery system exhibits synergistic antitumor effects by combining with a vaccinia viral vaccine. Int J Pharm 2008;350(1-2):27–34. [PubMed: 17897800]
11. Seo SH, Han HD, Noh KH, Kim TW, Son SW. Chitosan hydrogel containing GMCSF and a cancer drug exerts synergistic anti-tumor effects via the induction of CD8(+) T cell-mediated anti-tumor immunity. Clin Exp Metastasis. 2008
12. Zhang HM, Chen SR, Cai YQ, et al. Signaling mechanisms mediating muscarinic enhancement of GABAergic synaptic transmission in the spinal cord. Neuroscience 2009;158(4):1577–88. [PubMed: 19110040]
13. Temming K, Schiffelers RM, Molema G, Kok RJ. RGD-based strategies for selective delivery of therapeutics and imaging agents to the tumour vasculature. Drug Resist Updat 2005;8(6):381–402. [PubMed: 16309948]
14. Xie J, Shen Z, Li KC, Danthi N. Tumor angiogenic endothelial cell targeting by a novel integrin-targeted nanoparticle. Int J Nanomedicine 2007;2(3):479–85. [PubMed: 18019845]
15. Park JH, Kwon S, Nam JO, et al. Self-assembled nanoparticles based on glycol chitosan bearing 5beta-cholanic acid for RGD peptide delivery. J Control Release 2004;95(3):579–88. [PubMed: 15023468]
16. Ho MH, Wang DM, Hsieh HJ, et al. Preparation and characterization of RGD-immobilized chitosan scaffolds. Biomaterials 2005;26(16):3197–206. [PubMed: 15603814]

17. Kim JH, Kim YS, Park K, et al. Self-assembled glycol chitosan nanoparticles for the sustained and prolonged delivery of antiangiogenic small peptide drugs in cancer therapy. Biomaterials 2008;29(12):1920–30. [PubMed: 18289669]

18. Mitra A, Mulholland J, Nan A, McNeill E, Ghandehari H, Line BR. Targeting tumor angiogenic vasculature using polymer-RGD conjugates. J Control Release 2005;102(1):191–201. [PubMed: 15653145]

19. Mitra A, Coleman T, Borgman M, Nan A, Ghandehari H, Line BR. Polymeric conjugates of mono- and bi-cyclic alphaVbeta3 binding peptides for tumor targeting. J Control Release 2006;114(2): 175–83. [PubMed: 16889865]

20. Han HD, Shin BC, Choi HS. Doxorubicin-encapsulated thermosensitive liposomes modified with poly(N-isopropylacrylamide-co-acrylamide): drug release behavior and stability in the presence of serum. Eur J Pharm Biopharm 2006;62(1):110–6. [PubMed: 16183268]

21. Lu C, Kamat AA, Lin YG, et al. Dual targeting of endothelial cells and pericytes in antivascular therapy for ovarian carcinoma. Clin Cancer Res 2007;13(14):4209–17. [PubMed: 17634550]

22. Mangala LS, Zuzel V, Schmandt R, et al. Therapeutic Targeting of ATP7B in Ovarian Carcinoma. Clin Cancer Res 2009;15(11):3770–80. [PubMed: 19470734]

23. Hajitou A, Trepel M, Lilley CE, et al. A hybrid vector for ligand-directed tumor targeting and molecular imaging. Cell 2006;125(2):385–98. [PubMed: 16630824]

24. Mintz PJ, Cardo-Vila M, Ozawa MG, et al. An unrecognized extracellular function for an intracellular adapter protein released from the cytoplasm into the tumor microenvironment. Proc Natl Acad Sci U S A. 2009

25. Kim TJ, Ravoori M, Landen CN, et al. Antitumor and antivascular effects of AVE8062 in ovarian carcinoma. Cancer Res 2007;67(19):9337–45. [PubMed: 17909042]

26. Landen CN Jr, Chavez-Reyes A, Bucana C, et al. Therapeutic EphA2 gene targeting in vivo using neutral liposomal small interfering RNA delivery. Cancer Res 2005;65(15):6910–8. [PubMed: 16061675]

27. Landen CN Jr, Lu C, Han LY, et al. Efficacy and antivascular effects of EphA2 reduction with an agonistic antibody in ovarian cancer. J Natl Cancer Inst 2006;98(21):1558–70. [PubMed: 17077358]

28. Landen CN, Kinch MS, Sood AK. EphA2 as a target for ovarian cancer therapy. Expert Opin Ther Targets 2005;9(6):1179–87. [PubMed: 16300469]

29. Spannuth WA, Sood AK, Coleman RL. Angiogenesis as a strategic target for ovarian cancer therapy. Nat Clin Pract Oncol 2008;5(4):194–204. [PubMed: 18268546]

30. Donninger H, Bonome T, Radonovich M, et al. Whole genome expression profiling of advance stage papillary serous ovarian cancer reveals activated pathways. Oncogene 2004;23(49):8065–77. [PubMed: 15361855]

31. Apte SM, Fan D, Killion JJ, Fidler IJ. Targeting the platelet-derived growth factor receptor in antivascular therapy for human ovarian carcinoma. Clin Cancer Res 2004;10(3):897–908. [PubMed: 14871965]

32. Baker CH, Kedar D, McCarty MF, et al. Blockade of epidermal growth factor receptor signaling on tumor cells and tumor-associated endothelial cells for therapy of human carcinomas. Am J Pathol 2002;161(3):929–38. [PubMed: 12213721]

33. Hood JD, Bednarski M, Frausto R, et al. Tumor regression by targeted gene delivery to the neovasculature. Science 2002;296(5577):2404–7. [PubMed: 12089446]

34. Oba M, Fukushima S, Kanayama N, et al. Cyclic RGD peptide-conjugated polyplex micelles as a targetable gene delivery system directed to cells possessing alphavbeta3 and alphavbeta5 integrins. Bioconjug Chem 2007;18(5):1415–23. [PubMed: 17595054]

35. Kudo Y, Siriwardena BS, Hatano H, Ogawa I, Takata T. Periostin: novel diagnostic and therapeutic target for cancer. Histol Histopathol 2007;22(10):1167–74. [PubMed: 17616943]

36. Sood AK, Coffin JE, Schneider GB, et al. Biological significance of focal adhesion kinase in ovarian cancer: role in migration and invasion. Am J Pathol 2004;165(4):1087–95. [PubMed: 15466376]

37. Landen CN, Kim TJ, Lin YG, et al. Tumor-selective response to antibody-mediated targeting of alphavbeta3 integrin in ovarian cancer. Neoplasia 2008;10(11):1259–67. [PubMed: 18953435]

38. Lu C, Bonome T, Li Y, et al. Gene alterations identified by expression profiling in tumor-associated endothelial cells from invasive ovarian carcinoma. Cancer Res 2007;67(4):1757–68. [PubMed: 17308118]
39. Mangala LS, Han HD, Lopez-Berestein G, Sood AK. Liposomal siRNA for ovarian cancer. Methods Mol Biol 2009;555:29–42. [PubMed: 19495686]
40. Davis ME, Chen ZG, Shin DM. Nanoparticle therapeutics: an emerging treatment modality for cancer. Nat Rev Drug Discov 2008;7(9):771–82. [PubMed: 18758474]
41. Bartlett DW, Su H, Hildebrandt IJ, Weber WA, Davis ME. Impact of tumor-specific targeting on the biodistribution and efficacy of siRNA nanoparticles measured by multimodality in vivo imaging. Proc Natl Acad Sci U S A 2007;104(39):15549–54. [PubMed: 17875985]
42. McNeeley KM, Karathanasis E, Annapragada AV, Bellamkonda RV. Masking and triggered unmasking of targeting ligands on nanocarriers to improve drug delivery to brain tumors. Biomaterials 2009;30(23-24):3986–95. [PubMed: 19427688]
43. Bartlett DW, Davis ME. Physicochemical and biological characterization of targeted, nucleic acid-containing nanoparticles. Bioconjug Chem 2007;18(2):456–68. [PubMed: 17326672]
44. Lv H, Zhang S, Wang B, Cui S, Yan J. Toxicity of cationic lipids and cationic polymers in gene delivery. J Control Release 2006;114(1):100–9. [PubMed: 16831482]
45. Akhtar S, Benter I. Toxicogenomics of non-viral drug delivery systems for RNAi: potential impact on siRNA-mediated gene silencing activity and specificity. Adv Drug Deliv Rev 2007;59(2-3): 164–82. [PubMed: 17481774]
46. Hollins AJ, Omidi Y, Benter IF, Akhtar S. Toxicogenomics of drug delivery systems: Exploiting delivery system-induced changes in target gene expression to enhance siRNA activity. J Drug Target 2007;15(1):83–8. [PubMed: 17365277]
47. Akhtar S, Benter IF. Nonviral delivery of synthetic siRNAs in vivo. J Clin Invest 2007;117(12): 3623–32. [PubMed: 18060020]
48. Katas H, Alpar HO. Development and characterisation of chitosan nanoparticles for siRNA delivery. J Control Release 2006;115(2):216–25. [PubMed: 16959358]
49. Liu X, Howard KA, Dong M, et al. The influence of polymeric properties on chitosan/siRNA nanoparticle formulation and gene silencing. Biomaterials 2007;28(6):1280–8. [PubMed: 17126901]
50. Mangala, L.; Han, HD.; Lu, C., et al. In vivo vascular and tumor cell gene silencing with chitosan nanoparticles in ovarian carcinoma. AACR Meeting Abstracts 2008; 99th Annual Meeting; 2008. p. 5613
51. Gillan L, Matei D, Fishman DA, Gerbin CS, Karlan BY, Chang DD. Periostin secreted by epithelial ovarian carcinoma is a ligand for alpha(V)beta(3) and alpha(V)beta(5) integrins and promotes cell motility. Cancer Res 2002;62(18):5358–64. [PubMed: 12235007]

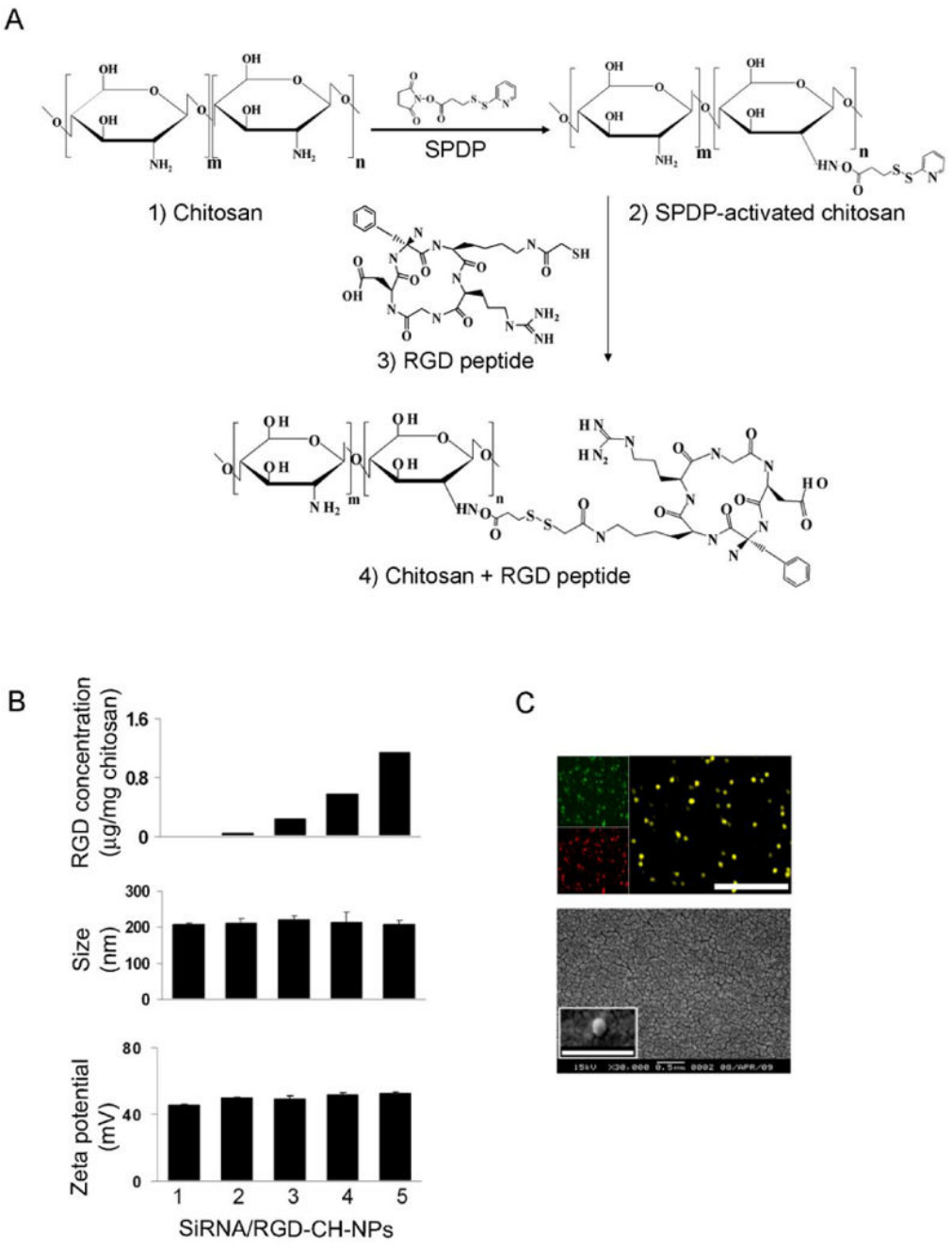


**Fig. 1.**

A, Conjugation of RGD to chitosan (CH). Physical properties of siRNA/RGD-CH-NPs. B (upper panel), RGD concentration in the siRNA/RGD-CH-NPs was calculated by measuring FITC intensity based on a calibration curve of standard concentration of FITC-labeled with RGD by fluorescence spectrophotometry. B (middle and lower panel), Size and zeta potential of siRNA/RGD-CH-NPs were measured by light scattering with a particle size analyzer and Zeta Plus, respectively. C, Incorporation of FITC-labeled RGD (green) and Alexa555 siRNA (red) into siRNA/RGD-CH-NPs was observed by fluorescence microscopy (magnification ×400, upper panel, scale bar: 1 μm). Morphology of siRNA/RGD-CH-NP 5

was examined by scanning electron microscopy (SEM, lower panel). Error bars represent s.e.m. *$p<0.05$.

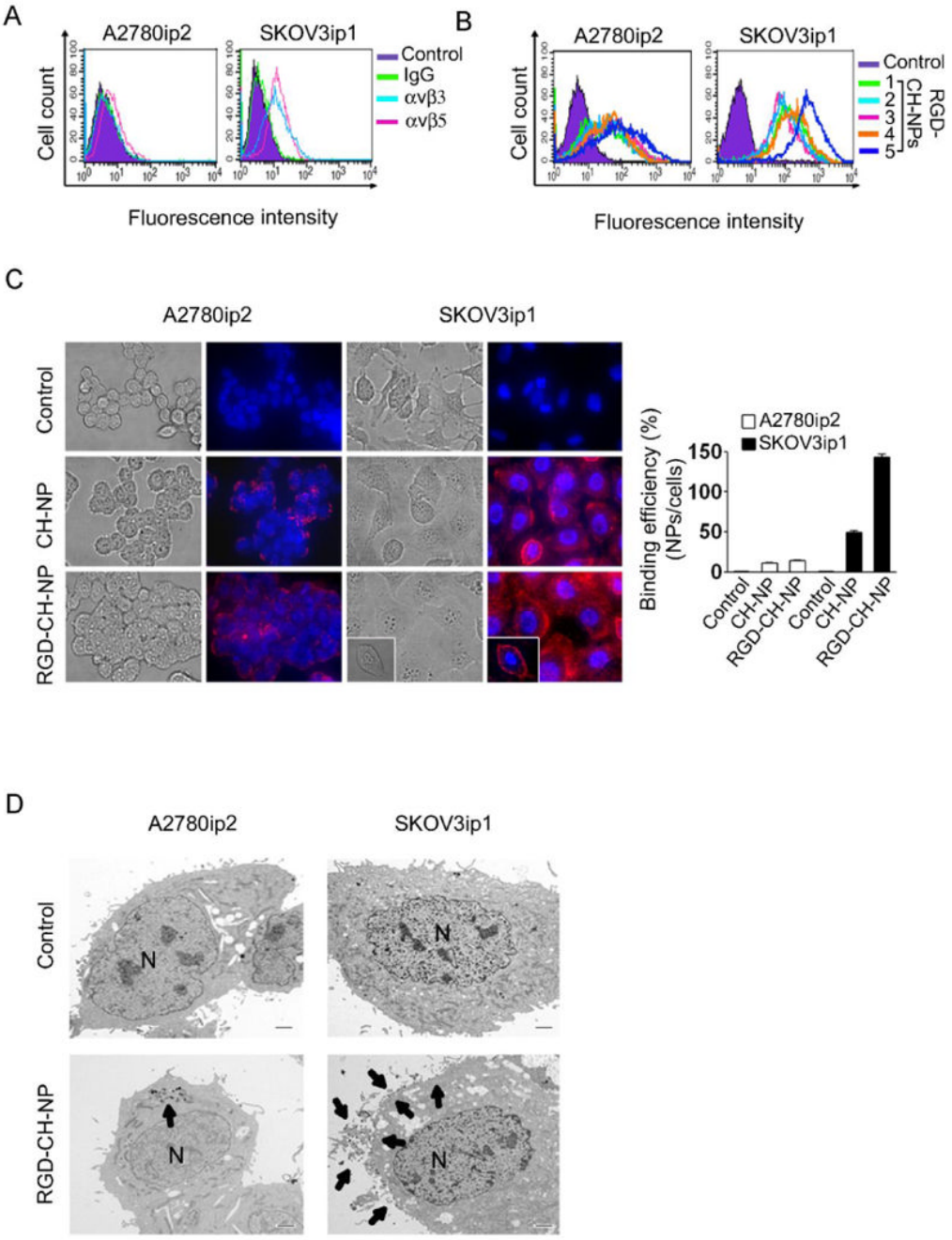


**Fig. 2.**

Binding of siRNA/RGD-CH-NPs against ovarian cancer cells *in vitro*. A, αvβ3 integrin expression on SKOV3ip1 or A2780ip2 cells by flow cytometry. Cells were incubated in RPMI-1640 supplemented with 10% fetal bovine serum at 37 °C for 24 hr, and then washed and incubated with 2.5 μg of either Alexa555 labeled siRNA/CH-NPs or siRNA/RGD-CH-NPs in PBS for 20 min at 4 °C. B, Binding of siRNA/RGD-CH-NPs with different concentrations of RGD peptide by flow cytometry. C, Binding of Alexa555 siRNA/RGD-CH-NPs and Alexa555 siRNA/CH-NP in SKOV3ip1 or A2780ip2 cells. Cells were fixed in a chamber slide using 4% paraformaldehyde and then nuclei (blue) were stained with Hoechst 33258 for 10 min, and binding was analyzed by fluorescence microscopy

(magnification ×200). Quantitative differences were analyzed by fluorescence intensity of Alexa555 (red)/Hoechst 33358 (blue). Error bars represent s.e.m. *$p$ <0.01. D, Binding of RGD-CH-NPs in SKOV3ip1 or A2780ip2 cells by TEM (N: nucleus, arrows: NPs, bar: 2 μm).

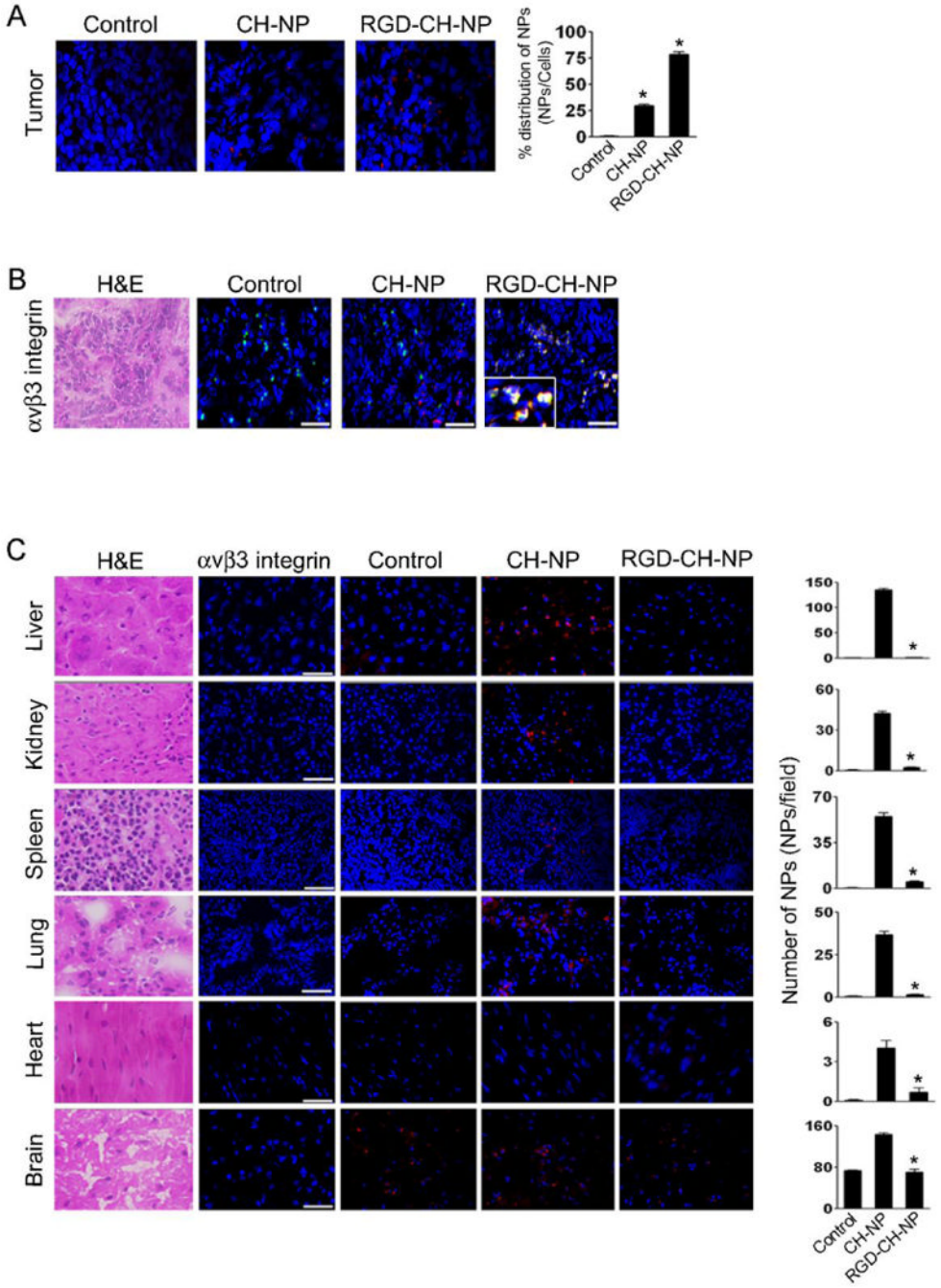


**Fig. 3.**

*In vivo* delivery of Alexa555 siRNA/RGD-CH-NP. Tumor and organ tissues were harvested after single injection of either control siRNA/CH-NP, Alexa555 siRNA/CH-NP, or Alexa555 siRNA/RGD-CH-NP into SKOV3ip1-bearing mice. Uptake efficiency was determined by the percentage of Alexa555 siRNA-labeled NPs in 5 random fields (original magnification ×200): A, Tumor and C, Various organs. B, Co-localization of Alexa 555 siRNA/RGD-CH-NP or CH-NP (red) and αvβ3 integrin (green) in tumor tissues (original magnification ×200). All of these analyses were recorded in 5 random fields for each slide. Error bars represent s.e.m. *$p$ <0.05.

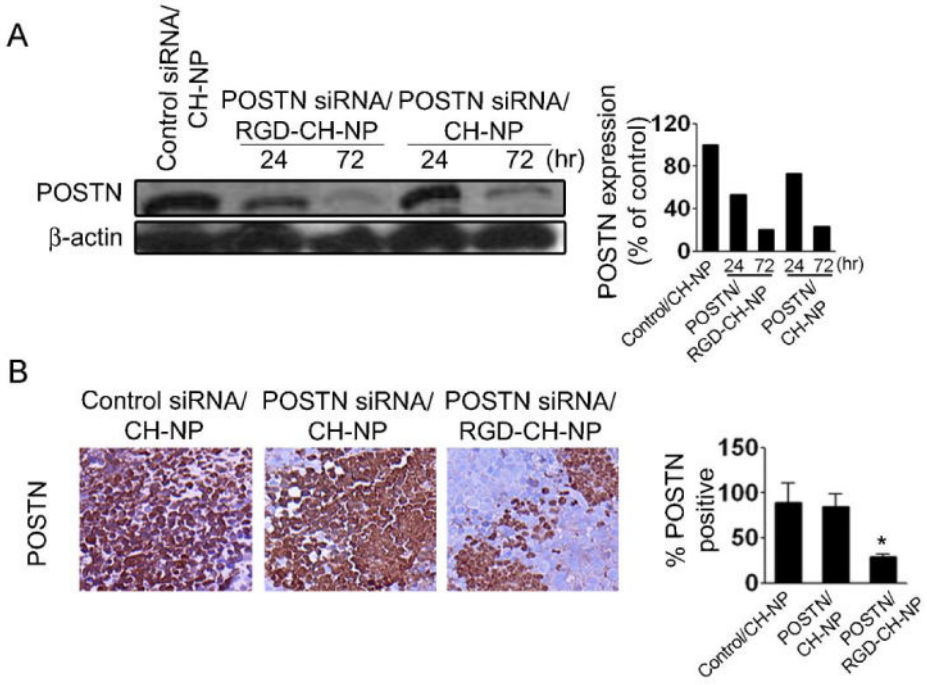


**Fig. 4.**

Effect of POSTN down regulation following intravenous injection of POSTN siRNA/RGD-CH-NP into SKOV3ip1-bearing mice. A, Western blot analysis was done for POSTN expression in tumor tissue (20 μg of protein used). Quantitative differences were determined by densitometry analysis. B, POSTN expression in tumor tissues was assessed by immunohistochemistry at 24 hr. All of these analyses were recorded in 5 random fields for each slide and quantitative difference was determined by positive/negative expression of cells for staining (magnification ×100). Error bars represent s.e.m. *$p$ <0.05.

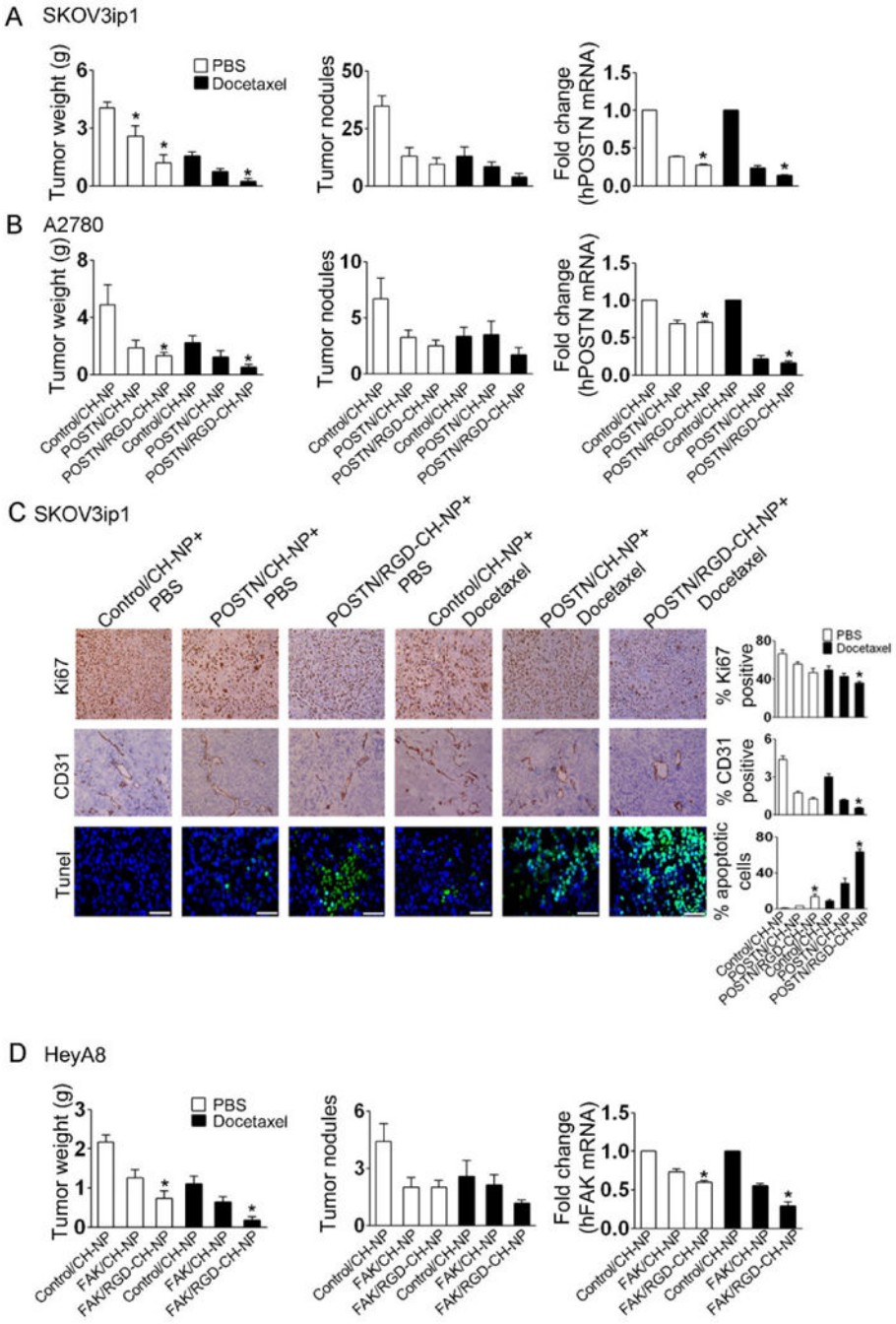


**Fig. 5.**

Effect of siRNA/RGD-CH-NP on ovarian cancer growth. Treatment was started 1 week after intraperitoneal injection of tumor cells into mice: A, SKOV3ip1 and B, A2780. Either siRNA-incorporated into CH-NP or RGD-CH-NP was given twice weekly at a dose of 150 μg/kg body weight through intravenous injection. Docetaxel was diluted in PBS and injected intraperitoneally once per week, at a dose of 100 μg, in 200 μl of PBS. Treatment was continued until mice in any group became moribund (typically 4 to 5 weeks depending on tumor cell). The fold change in levels of POSTN mRNA represents the mean of triplicate experiments by qRT-PCR. C, Immunohistochemistry for cell proliferation (Ki67, magnification ×100), microvessel density (CD31, magnification ×100), and TUNEL (bar: 50

μm) was performed on SKOV3ip1-tumor tissues following treatment with POSTN siRNA/RGD-CH-NP or CH-NP. All of these analyses were recorded in 5 random fields for each slide. D, HeyA8 tumor model treated with FAK siRNA/RGD-CH-NP or CN-NP. The fold change in FAK mRNA levels represents the mean of triplicate experiments by qRT-PCR. Error bars represent s.e.m. $*p < 0.05$.

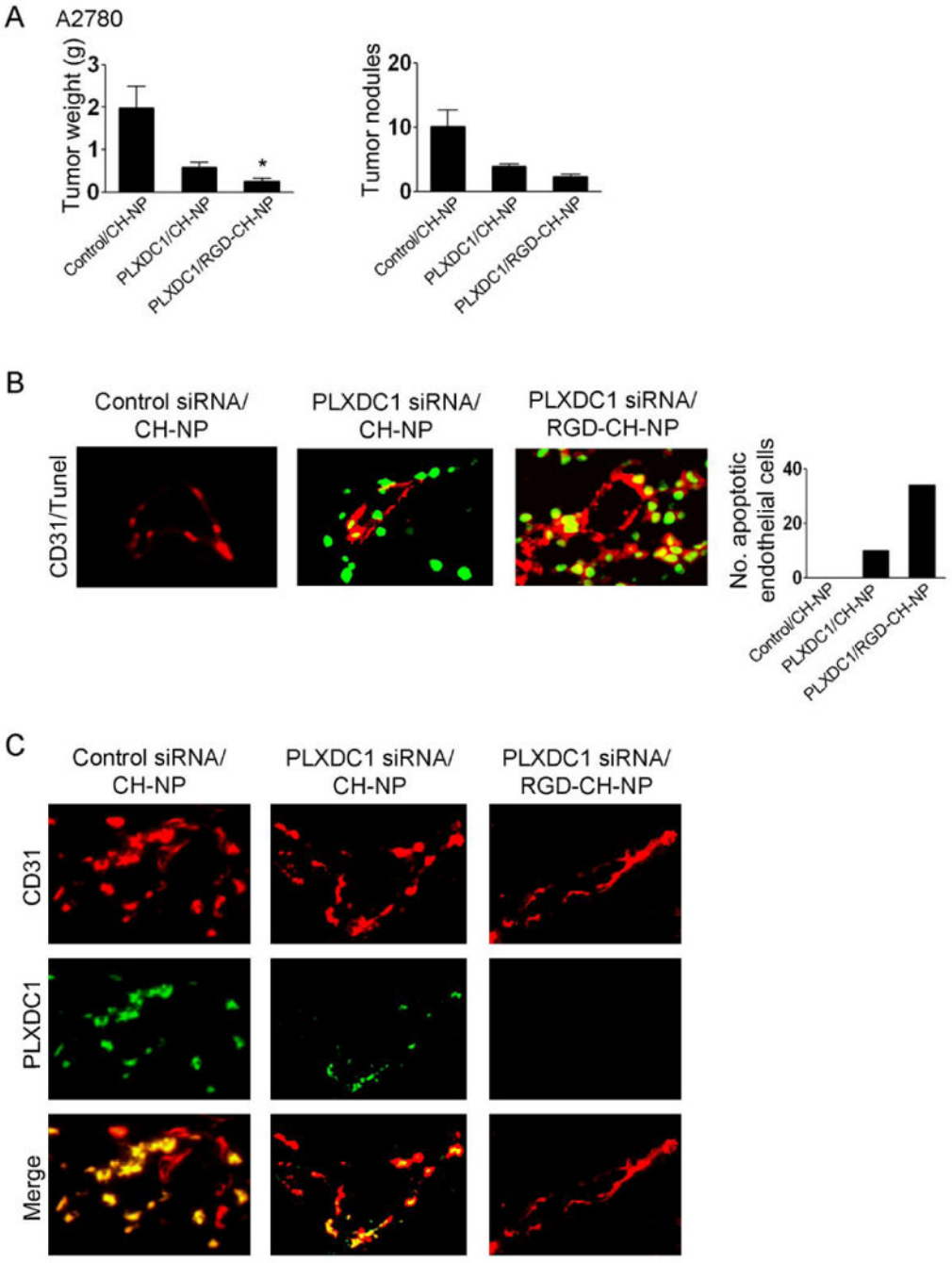


**Fig. 6.**

Therapeutic efficacy of siRNA/RGD-CH-NP against A2780-bearing mice. A, Anti-tumor effect of mouse PLXDC1 siRNA/RGD-CH-NP or CH-NP in the A2780 tumor model. Error bars represent s.e.m. *$p$ <0.05. B, Effect of PLXDC1 siRNA/RGD-CH-NP treatment on apoptosis in the tumor vasculature. Tumor sections were stained with CD31 (red) and TUNEL (green) using double immunofluorescence staining. Colocalization of endothelial cells undergoing apoptosis appears yellow (magnification ×400). All of these analyses were recorded in 5 random fields for each slide and quantitative differences were analyzed by positive expression of TUNEL/CD31. C, Tumor sections were stained with CD31 (red) and

PLXDC1 (green) using immunofluorescence staining to examine PLXDC1 silencing in the tumor vasculature (magnification ×400).